

**Dynamical phase trajectories for relativistic nuclear collisions**I. C. Arsene,<sup>1</sup> L. V. Bravina,<sup>1</sup> W. Cassing,<sup>2</sup> Yu. B. Ivanov,<sup>3</sup> A. Larionov,<sup>2,3</sup> J. Randrup,<sup>4</sup> V. N. Russkikh,<sup>3</sup>  
V. D. Toneev,<sup>5</sup> G. Zeeb,<sup>6</sup> and D. Zschesche<sup>6,7</sup><sup>1</sup>*Fysisk Institutt, Universitet i Oslo, N-0316 Oslo, Norway*<sup>2</sup>*Institut für Theoretische Physik, Justus-Liebig-Universität, Gießen, D-35392 Germany*<sup>3</sup>*Kurchatov Institute, RU-123182 Moscow, Russia*<sup>4</sup>*Nuclear Science Division, Lawrence Berkeley National Laboratory, Berkeley, California 94720, USA*<sup>5</sup>*Joint Institute for Nuclear Research, RU-141980 Dubna, Russia*<sup>6</sup>*Institut für Theoretische Physik, Johann Wolfgang Goethe-Universität, Frankfurt, D-60438 Germany*<sup>7</sup>*Instituto de Física, Universidade Federal do Rio de Janeiro, 21941-972 RJ, Brazil*

(Received 19 September 2006; published 12 March 2007)

Central collisions of gold nuclei are simulated by several existing models and the central net baryon density  $\rho$  and the energy density  $\varepsilon$  are extracted at successive times for beam kinetic energies of 5–40 GeV/nucleon. The resulting trajectories in the  $(\rho, \varepsilon)$  phase plane are discussed from the perspective of experimentally exploring the expected first-order hadronization phase transition with the planned FAIR at GSI or in a low-energy campaign at the Relativistic Heavy Ion Collider.

DOI: [10.1103/PhysRevC.75.034902](https://doi.org/10.1103/PhysRevC.75.034902)

PACS number(s): 25.75.Nq

**I. INTRODUCTION**

One of the major goals of high-energy heavy-ion research is to explore the properties of strongly interacting matter, particularly its phase structure [1]. The regions of temperature and baryon density that can be accessed depend on the collision energy. Thus systems with a very small net baryon density but rather high temperature are formed at the Relativistic Heavy Ion Collider (RHIC) [2] [ $s_{NN} \simeq (200 \text{ GeV})^2$ ], while it is expected that the creation of the highest possible baryon densities would occur at more moderate collision energies ( $s_{NN} \simeq (6 \text{ GeV})^2$  [3]), such as those becoming available at the planned Facility for Antiproton and Ion Research (FAIR) [4] or at the low-energy end of RHIC.

Our understanding of the quantum chromodynamics (QCD) phase diagram is best developed at vanishing chemical potential,  $\mu_C = 0$ , where lattice QCD calculations are most easily carried out. The most recent results indicate that the transformation from a low-entropy hadron resonance gas to a high-entropy quark-gluon plasma occurs smoothly as the temperature is raised, with no real phase transition being present [5].

However, at zero temperature most models predict the occurrence of a first-order phase transition when the density is raised [6], though no firm results are yet available for the corresponding value of the chemical potential,  $\mu_0$ . However, if the  $T = 0$  transformation is in fact of first order, one would expect the phase boundary to extend into the region of finite temperature and terminate at a certain critical endpoint,  $(\mu_c, T_c)$  [6]. Indeed, recent lattice QCD results [7] suggest the presence of such a first-order phase transition line and an associated critical end-point, though its precise location is not yet determined.

FAIR, which is under construction at GSI in Germany, will make it possible to create compressed baryonic matter in the laboratory, matter with a high net baryon density. The increasing interest in this area of physics is underscored

by the recent proposal for a low-energy campaign at RHIC aimed at the identification of the critical point [8] and by current discussions about the feasibility of searching for the mixed phase at the Joint Institute for Nuclear Research (JINR) Nuclotron [9].

To assess the prospects for using these facilities to explore the phase structure it is important to know what thermodynamic environments are being generated in the bulk of the collision systems at the various bombarding energies available. For this purpose, we employed a number of existing models to simulate central collisions of gold nuclei in the beam energy range anticipated at FAIR (5–40 GeV/nucleon) and then extracted key information about the bulk environments generated in the course of a collision.

**II. THE INFORMATION EXTRACTED**

Generally, the systems involved in a high-energy nuclear collision evolve rapidly in time and, furthermore, they are far from being uniform in space. The former feature prevents equilibrium from being fully established, whereas the latter feature invalidates the familiar thermodynamic relations that pertain to bulk matter. As a consequence, dynamical simulation models are indispensable in the exploration of these processes.

However, within a given microscopic transport model, it is possible to extract the characteristics of the local environment at any point in space and time and on this basis ascertain the degree of local equilibrium achieved and extract the corresponding local characteristics.

Such a study was first made by Dorso *et al.* [10], who calculated the breakup of an initially compressed and heated nucleus and extracted its thermodynamic phase evolution. This analysis showed that the bulk of the system entered the spinodal region associated with the first-order nuclear liquid-gas phase transition. Furthermore, the resulting fragmentation pattern exhibited signs of filamentation, a general characteristic feature of spinodal phase decomposition.

As an instructive reference case for our present study, we consider central collisions of two gold nuclei and focus on the physical conditions at the center of the system. Thus, in the center-of-mass (c.m.) frame, we consider only a small region around the origin,  $\mathbf{r} = (0, 0, 0)$ , and then seek to characterize the physical environment there as it evolves in the course of time.

We are particularly interested in the net baryon density  $\rho(t) = \rho_B(t) - \rho_{\bar{B}}(t)$  and the energy density  $\varepsilon(t)$ . The local stress tensor is also of interest but will not be examined here. Because we focus on the center of the system, there is no collective flow by symmetry. (Although this is strictly true only on the average, each individual event might display some flow at the origin, but this possibility is unimportant and may be safely disregarded.) We do not wish to engage in a technical discussion of how these quantities can be extracted in the various models but refer the reader to the relevant literature cited for each particular model. We only note here that in numerical treatments that employ a grid in position space, such as fluid dynamics, these values can simply be read off at the appropriate lattice site (the origin, in the present case), whereas methods that represent the dynamical state of the system in terms of individual (test) particles must resort to an average over a suitably small test volume  $\Delta V$  around the origin. (Due to the strong Lorentz contraction early on, the test volume must initially be sufficiently thin; a typical choice would be  $|x|, |y|, \gamma_{\text{cm}}|z| \leq 2$  fm, where  $\gamma_{\text{cm}}$  is the Lorentz factor associated with the initial nuclear motion in the c.m. frame. However, as the longitudinal expansion progresses and the system grows increasingly dilute, it may improve the sampling statistics to stretch the test box.)

It is important to note that both  $\rho$  and  $\varepsilon$  have well-defined values at all times. In particular, their extraction does not require that local thermal equilibration has been reached. This is one advantage of considering these particular observables for the present study. However, of course, their thermodynamic relevance does depend on the degree of local equilibration achieved, as reflected principally in the isotropy of the pressure tensor.

In each individual model, it may be possible to also extract local thermodynamic quantities, such as temperature  $T$ , chemical potential  $\mu$ , or entropy density  $\sigma$ , but although most extraction methods can be cast in sufficiently general terms to make them applicable also to nonequilibrium scenarios, those quantities have physical meaning only in equilibrium. Furthermore, importantly, even if equilibrium is reached, identical values of  $\rho$  and  $\varepsilon$  will generally lead to different values for those thermodynamic quantities from one model to the other, due to their differences in mean fields and degrees of freedom.

By contrast, the mechanical quantities  $\rho$  and  $\varepsilon$  are inherently more robust variables because they are subject to local conservation laws. For example, in ideal fluid dynamics the conservation of four-momentum is expressed as  $\partial_\mu T^{\mu\nu} = 0$ , whereas the conservation of baryon charge is expressed by the continuity equation  $\partial_\mu j^\mu = 0$ . Because the various dynamical models generally abide by these basic conservation laws, they will have a tendency to yield similar results for the

corresponding quantities. By asking about the behavior of such conserved observables we may therefore expect to obtain relatively robust answers. [Of course, for the purpose of discriminating between models (which is *not* our purpose here), it would probably be better to consider observables that are more sensitive to the specific model ingredients.]

To further underscore the qualitative difference between “mechanical” or “dynamical” quantities such as  $\rho$  and  $\varepsilon$  and “thermodynamical” quantities such as  $\mu$  and  $T$ , we note that the above-mentioned conservation laws guarantee that the local energy or (baryon) charge density cannot change without the occurrence of a suitable amount of energy or charge transport, which requires some time. By contrast, there are no such conservation laws restricting the rate of change of the local temperature or entropy or chemical potential, which can change essentially instantaneously as a result of local reaction processes, such as ionization or chemical bonding. (Although such phenomena may well offer useful signals of the hadronization phase transition, which can be viewed as some sort of bonding, they are not of interest for the present study.)

A further advantage of considering the variables  $\varepsilon$  and  $\rho$  rather than  $T$  and  $\mu$  is that the equation of state, i.e., the pressure  $p(\varepsilon, \rho)$ , is then always a single-valued function, whereas this is not always the case for  $p(T, \mu)$ . Indeed, precisely when a first-order phase transition is present, the bulk pressure (i.e., the pressure of a spatially uniform system),  $p(T, \mu)$ , is multivalued throughout the region of phase coexistence. Because of this feature, if the phase trajectory were represented as  $(\mu(t), T(t))$ , it would exhibit a rather complex behavior as the expansion drives the system through the phase coexistence region, thus complicating the analysis considerably. This problem is not encountered in the  $(\rho(t), \varepsilon(t))$  representation, where the phase trajectory has a regular behavior throughout. This makes it easy, for example, to see how long time will be spent in the spinodal phase-coexistence region where bulk matter is mechanically unstable.

### III. PHASE DIAGRAM

The most relevant features of the  $\rho$ - $\varepsilon$  phase plane are depicted in Fig. 1. At a given density  $\rho$ , the zero-temperature compressional energy,  $\varepsilon_{T=0}(\rho)$ , provides a lower bound on the energy density  $\varepsilon$ , so the accessible region is correspondingly limited. A useful reference is provided by the phase-coexistence boundaries associated with a recently constructed equation of state [11] that has a first-order phase transition at all baryon densities. Also shown is the corresponding boundary of a schematic equation of state that has a critical point at a finite density, as is now generally expected. Although these boundaries are only approximate and illustrative, they may serve as convenient references on the plots of the calculated phase trajectories.

Figure 1 also shows where the hadronic freeze-out occurs [12]. This representation brings out the fact that the freeze-out environments are quite different from those near the phase coexistence boundary, thus underscoring the importance of studying the propagation and survival of any proposed phase-transition signals through freeze-out.

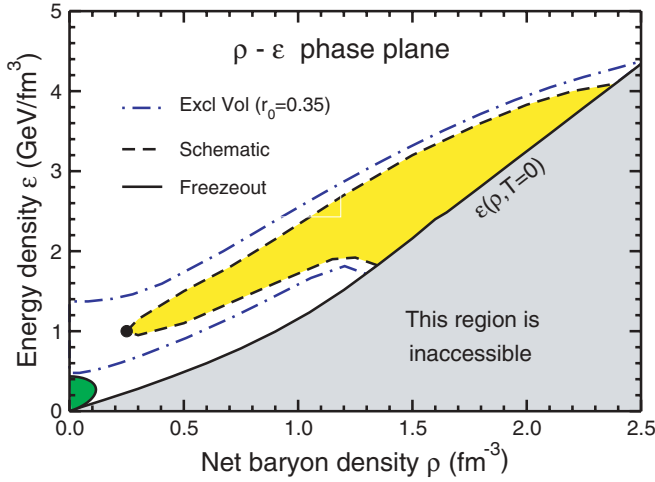


FIG. 1. (Color online) The  $\rho$ - $\epsilon$  phase plane used for representing the extracted dynamical evolution of the central environment in Au+Au collisions. The energetically accessible region is bounded from below by the zero-temperature compressional energy density  $\epsilon_{T=0}(\rho)$ . The hadronic freeze-out is indicated at the lower left [2]. The phase coexistence region obtained in Ref. [11] on the basis of an excluded volume is delineated by the outer contour, whereas the inner contour, which depicts a schematic boundary with a critical point, will serve as a reference for the phase trajectories.

### A. Isentropic expansion

To establish an instructive framework for understanding the results obtained with the various dynamical models, we consider first adiabatic expansions. For this we use the hadronic chiral flavor-SU(3) model [13]. This model is based on a chiral hadronic SU(3) Lagrangian that incorporates and couples the complete set of baryons from the lowest flavor-SU(3) octet, the entire multiplets of scalar, pseudoscalar, vector, and axial vector mesons, as well as baryon resonance states [13–15]. These hadrons have various types of interaction that endow them with effective masses and induce spontaneous chiral symmetry breaking as well as scale breaking via a dilaton field. The parameters of the model are fixed by symmetry considerations, hadronic vacuum observables, or nuclear matter saturation properties. The model provides a satisfactory description of both finite nuclei and neutron stars [13,16,17] and, furthermore, it has been used for fluid-dynamical studies of the space-time evolution and HBT radii in relativistic nuclear collisions [14].

With the baryon resonance couplings chosen suitably, the phase diagram of the SU(3) model is in qualitative agreement with the picture obtained from lattice results [18], as illustrated by the corresponding phase boundary in Fig. 2. (But it is seen to differ quantitatively from the schematic reference boundary discussed above—a useful reminder of that fact that the phase boundary is still rather poorly understood.) Furthermore, phase trajectories that are consistent with the phase diagram of the model can be obtained by performing adiabatic expansions. Such expansions conserve the entropy per net baryon and that condition in turn yields a unique trajectory in the  $\rho$ - $\epsilon$  phase plane, once the initial phase point  $(\rho_i, \epsilon_i)$  has been specified.

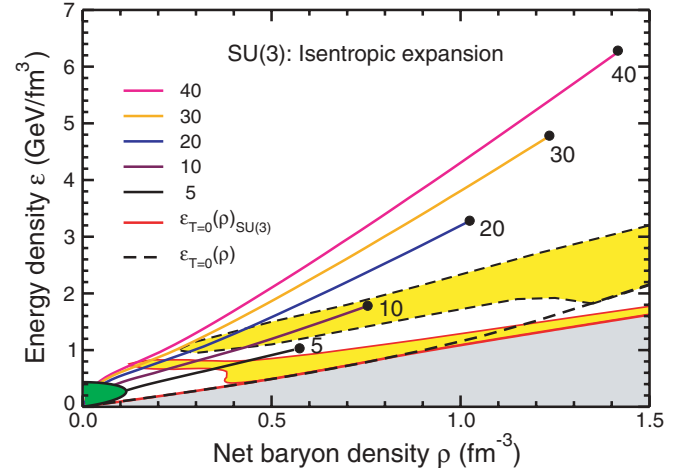


FIG. 2. (Color online) The chiral hadronic SU(3) model: The energetically inaccessible region (gray area) and the phase-coexistence region (shaded area within solid boundary) are shown together with the corresponding quantities for the schematic equation of state displayed in Fig. 1. Also shown are the phase trajectories  $(\rho, \epsilon)$  resulting from adiabatic expansions starting from counterstreaming Lorentz-contracted nuclei at the indicated beam kinetic energies  $E_0$  (A GeV).

A simple but rough estimate of the initial conditions can be obtained by assuming that the very early dynamics is dominated by the interpenetration of the two Lorentz-contracted nuclei. Then the early baryon density (in the c.m. frame) is  $\rho_i = 2\gamma_{\text{cm}}\rho_0$ , where  $\rho_0 \approx 0.15 \text{ fm}^{-3}$  is the normal nuclear saturation density present in the nuclear interior and  $\gamma_{\text{cm}}$  is the Lorentz factor of the nuclei in the c.m. frame,  $\gamma_{\text{cm}}^2 = 1 + E_0/2m_N$ , where  $E_0$  is the beam kinetic energy per nucleon for a stationary target. In the c.m., the energy per baryon is  $\gamma_{\text{cm}}m_N$ , so the energy density is  $\epsilon_i = \gamma_{\text{cm}}m_N\rho_i = 2\gamma_{\text{cm}}^2m_N\rho_0 = (2m_N + E_0)\rho_0$ . The resulting phase trajectories  $(\rho, \epsilon)$  are depicted in Fig. 2. They are straight lines through the phase-coexistence region, whereas they are slightly convex above it and slightly concave below it.

As we shall see, the corresponding adiabatic compression (obtained by following these phase trajectories in the opposite direction) are remarkably similar to the calculated dynamical paths through the early nonequilibrium stage when counterstreaming dominates, whereas the subsequent dynamical expansion trajectories generally exhibit gentler slopes.

## IV. DYNAMICAL RESULTS

We have employed a number of different dynamical models in this comparative study. Because they have been already described in the literature we present only brief characterizations here and concentrate on the resulting phase trajectories.

### A. Three-fluid hydrodynamics

We first consider the three-fluid model [3], which treats two baryon-rich fluids originating with the incoming nuclei and a baryon-free fluid created through the collisions among

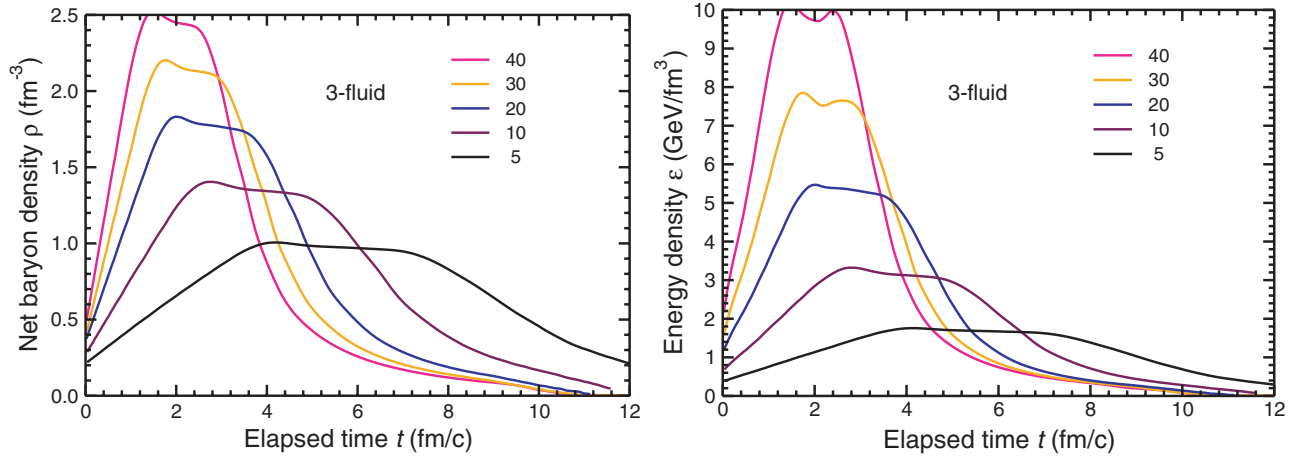


FIG. 3. (Color online) The time evolution of the net baryon density  $\rho(t)$  (left) and the total energy density  $\varepsilon(t)$  (right) at the center of a head-on Au+Au collision for various bombarding energies (indicated in A GeV), in the three-fluid model.

the [equation-of-state- (EOS) dependent] constituents of the first two fluids. The evolution of the baryon-free fluid is delayed by a formation time  $\tau$ , during which it neither thermalizes nor interacts with the baryon-rich fluids. After its formation, it starts to interact with the baryon-rich fluids and quickly thermalizes. With a purely hadronic equation of state, this model was used to carry out a systematic analysis of various observables at incident energies between few and about 160 GeV/nucleon, and a comparison with results of transport models was made as well.

A large body of data was well reproduced, including proton and pion rapidity distributions, proton transverse-mass spectra,  $\Lambda$  and  $\bar{\Lambda}$  rapidity distributions, protons and pion elliptic flow (except for the proton  $v_2$  at 40 A GeV), multiplicities of pions, positive kaons,  $\phi$  mesons, hyperons, and antihyperons, including multistrange particles. This agreement is achieved at the expense of substantial enhancement of the interflow friction, as compared to that estimated from free hadronic cross sections. Problems were met in reproducing the transverse flow [19], e.g., the directed flow requires a softer EOS at the top energies of the Alternating Gradient Synchrotron (AGS) and the Super Proton Synchrotron (SPS). This failure appears to suggest that the employed purely hadronic equation of state is too hard and thus leaves room for softening due to deconfinement. Further studies are in progress [20].

The evolutions of the central values of  $\rho$  and  $\varepsilon$  in head-on Au+Au collisions obtained with the three-fluid model are depicted in Fig. 3 for beam kinetic energies ranging from 5 to 40 GeV/nucleon. At each beam energy,  $\rho(t)$  and  $\varepsilon(t)$  are approximately proportional and exhibit a rapid growth as the two Lorentz-contracted nuclei interpenetrate, followed by a somewhat slower decrease reflecting the subsequent expansion. As the beam energy is increased, the entire history is being compressed in time.

The separate evolutions  $\rho(t)$  and  $\varepsilon(t)$  are then combined in Fig. 4 to yield the corresponding dynamical phase trajectory [ $\rho(t)$ ,  $\varepsilon(t)$ ]. At each beam energy, the return path depicting the expansion lies below the early (outwards) path, although

the two paths generally differ only relatively little. As was the case for the adiabatic results considered above, each such “common” path is fairly straight and its slope increases steadily with the beam energy. For the lowest energy, 5 A GeV, the trajectory just makes it to the hadronic boundary of the schematic phase coexistence region, whereas the next energy, 10 A GeV, already produces a turning point on the plasma side beyond the schematic phase coexistence region. Thus, of the trajectories shown, this one spends the longest time traversing the phase coexistence region during the expansion phase, and the crossing time becomes ever shorter as the beam energy is raised.

It should be recalled that the projection onto the  $(\rho, \varepsilon)$  phase plane requires no assumption about local equilibrium (which is very convenient for the purpose of the present study). In fact, generally, the central conditions are far from equilibrated during the early part of the collision. Therefore, before any thermodynamical implications could be made it would be

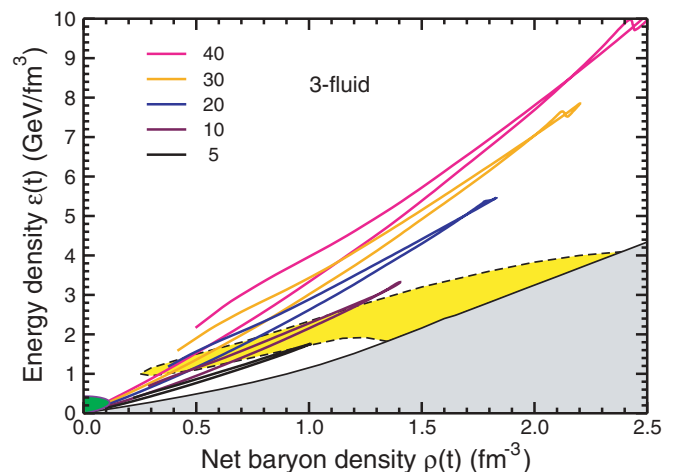


FIG. 4. (Color online) The phase trajectories  $(\rho(t), \varepsilon(t))$  for the three-fluid collisions addressed in Fig. 3, together with the schematic reference phase boundary depicted in Fig. 1.

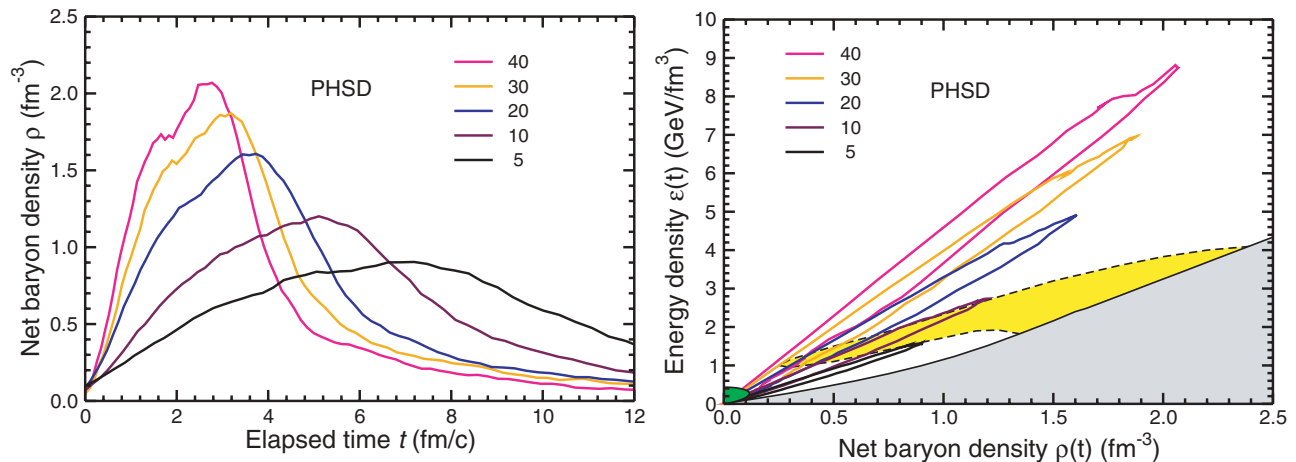


FIG. 5. (Color online) The time evolution of the central net baryon density  $\rho(t)$  (left) and the corresponding phase trajectory ( $\rho(t), \epsilon(t)$ ) (right) at the center of a head-on Au+Au collision at various bombarding energies (indicated in  $A$  GeV), in the PHSD model, together with the schematic reference phase boundary depicted in Fig. 1.

necessary to carefully analyze the degree of equilibrium attained at any particular time of interest.

### B. Parton-hadron string dynamics

We now consider a number of microscopic transport models. The first one is a recently extended version of the HSD model [21] called PHSD (parton-hadron-string dynamics) [22]. This version includes additionally an early partonic phase with an equation of state from lattice QCD and quasiparticle properties for quarks, antiquarks, and gluons that have been obtained from fits to lattice results [23]. On the hadronic side it treats explicitly the familiar baryon octet and decuplet and selected higher resonances as well as their antiparticles. On the meson side it includes the pseudoscalar and vector meson nonets as well as some higher meson resonances ( $a_1$ , etc.). Hadrons of even higher mass are treated as “strings” that reflect the continuum excitation spectrum of mesons or baryons. Because the results from the novel PHSD are very similar to those from HSD (without partonic phase) for central Au+Au collisions below about 25  $A$  GeV we omit a more detailed description of the PHSD model here.

We recall that the HSD model has been extensively compared to experimental data from nucleus-nucleus reactions for energies of 1  $A$  GeV to the top RHIC energies [ $s_{NN} = (200 \text{ GeV})^2$ ] for hadrons made up from the light  $u, d$  quarks, strange hadrons [24,25] as well as open and hidden charm [26]. It compares rather well with data (and the URQMD model described below) for observables such as hadron rapidity distributions [24] but falls somewhat low in the  $K^+/\pi^+$  ratio at top AGS and FAIR energies. Collective flow observables [ $v_1(y), v_2(y)$ ] are reproduced rather well in the energy regime of the Schwerionen Synchrotron (SIS) and AGS [27] due to momentum-dependent scalar and vector self-energies for the baryons. However, the transverse slope of kaons and antikaons is underestimated for bombarding energies above about 5  $A$  GeV in central Au+Au collisions, which has lead

to the suggestion that a “new phase of matter” or “partonic degrees of freedom” should already be encountered at top AGS energies [28].

The results obtained with PHSD are shown in Fig. 5. [Here and for the subsequent models, we do not show  $\epsilon(t)$  because it is approximately proportional to  $\rho(t)$ .] The time evolution of the densities  $\rho(t)$  are remarkably similar to those obtained with the three-fluid model discussed above, but it can be seen that PHSD leads to somewhat smaller compressions, particularly at higher collision energies.

The PHSD phase trajectories are therefore also rather similar to those obtained with the three-fluid model, except for somewhat smaller compressions and excitations at the highest energies. (We may also note that both models yield a curious double-hump structure of the density maxima, particularly at the higher energies.) Furthermore, at each energy, the inward path is rather similar to the outward path, though the differences are larger than those obtained with the three-fluid model. We also note that the 5  $A$  GeV phase trajectory turns around just at the hadronic border of the schematic phase coexistence region (as for the three-fluid model), whereas the 10 GeV/nucleon phase trajectory turns around at just the schematic plasma phase boundary of this region.

### C. Ultrarelativistic quantum molecular dynamics

The ultrarelativistic quantum molecular dynamics model (URQMD) [29,30] is a microscopic model used to simulate (ultra-)relativistic heavy-ion collisions in the energy range from the BEVALAC and SIS up to AGS, SPS, and RHIC allowing for a consistent calculation of excitation functions. Its main goals are to gain understanding of the various physical phenomena within a single transport model, including creation of dense hadronic matter at high temperatures, properties of nuclear matter,  $\Delta$  and resonance matter, mesonic matter and antimatter, creation and transport of rare particles in hadronic matter, creation, modification and destruction of strangeness in matter, and emission of electromagnetic probes.

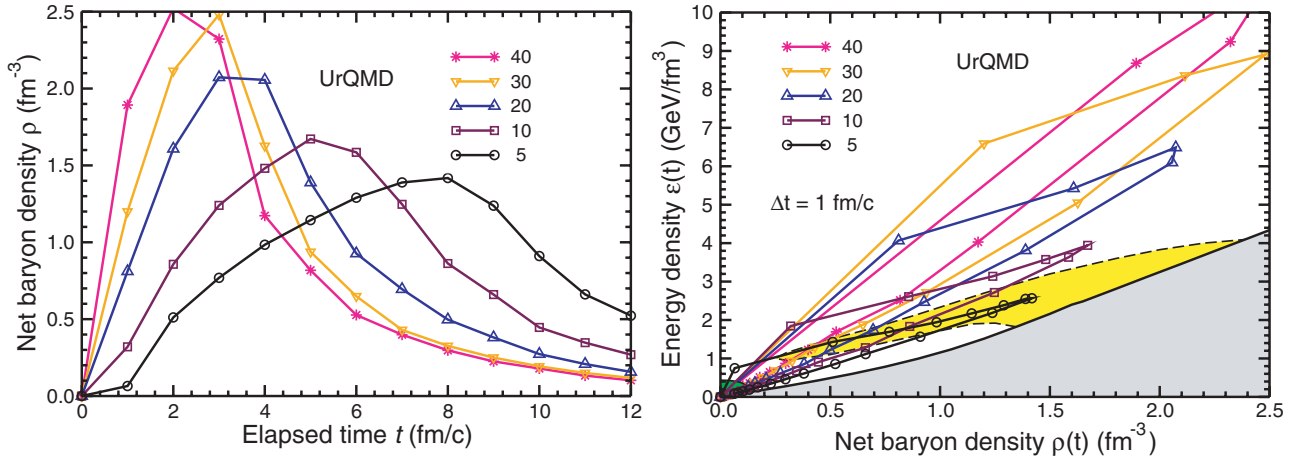


FIG. 6. (Color online) The time evolution of the central net baryon density  $\rho(t)$  (left) and the corresponding phase trajectory  $(\rho(t), \varepsilon(t))$  (right) at the center of a head-on Au+Au collision at various bombarding energies (indicated in  $A$  GeV), in the URQMD model, together with the schematic reference phase boundary depicted in Fig. 1. The symbols on the curves are separated by  $\Delta t = 1$  fm/c.

The initial projectile and target nuclei are modeled according to the Fermi gas ansatz and the nucleons are represented by Gaussian-shaped density distributions. URQMD includes in its collision term 55 different baryon species with masses up to 2.25 GeV, 32 meson species (including strange meson resonances) that are supplemented by their corresponding antiparticle, and all isospin-projected states. All these states can be produced in string decays,  $s$ -channel collisions, or resonance decays. For excitations with masses higher than 2 GeV a string picture is used. The hadron-hadron collisions are performed stochastically like in the cascade models. The elementary cross sections are fitted to available  $pp$ ,  $\pi p$  data and the isospin symmetry are used whenever possible to reduce the number of individual cross sections. For the interactions where no experimental data exist (e.g., hyperon-baryon resonance scattering), the additive quark model is used.

The interactions are based on a nonrelativistic density-dependent Skyrme-type equation of state with additional Yukawa and Coulomb potentials at low energies. However, no potentials were used in the present calculations. For the high-energy regime and baryon-antibaryon annihilation, URQMD uses a string model similar to the Lund model [31,32]. The strings, or the color tubes, are first formed in the high-energy  $hh$  interactions and then fragment into hadrons and new strings according to the Lund fragmentation procedure. For the ultrahigh energies (top SPS energies and beyond) the formation of jets is also introduced into the model.

The URQMD results are shown in Fig. 6. While the time evolutions of the densities  $\rho(t)$  and  $\varepsilon(t)$  are qualitatively similar to those obtained with the other models discussed, the URQMD compressions are somewhat higher than those of PHSD and more similar to the quark-gluon string model (QGSM) results (see below). A likely reason for this is that neither URQMD nor QGSM has any constraint on the closest approach between two baryons, whereas both the three-fluid model and PHSD have some repulsion.

#### D. Quark-gluon string model

The QGSM [33–36] incorporates partonic and hadronic degrees of freedom and is based on Gribov-Regge theory (GRT) [37], accomplished by a string phenomenology of particle production in inelastic hadron-hadron collisions. To also describe hadron-nucleus and nucleus-nucleus collisions, the cascade procedure of multiple secondary interactions of hadrons was implemented. The QGSM incorporates string fragmentation, formation of resonances, and rescattering of hadrons but simplifies some nuclear effects (for example, it neglects the mean fields).

As independent degrees of freedom the QGSM includes the octet and decuplet baryons, the octet and nonet vector and pseudoscalar mesons, and their antiparticles. The initial momenta and positions of nucleons inside the nuclei are generated in accordance with the Fermi momentum distribution and the Woods-Saxon density distribution, respectively. Pauli blocking of occupied final states is taken into account.

Strings in the QGSM can be produced as a result of the color exchange mechanism or, like in diffractive scattering, momentum transfer. The Pomeron, which is a pole with an intercept  $\alpha_P(0) > 1$  in GRT, corresponds to the cylinder-type diagrams. The inclusive spectra in the QGSM have automatically the correct triple-Regge limit for the Feynman variable  $x \rightarrow 1$  and double-Regge limit for  $x \rightarrow 0$  and satisfy all conservation laws. The particular stages of the collision model, namely (i) initialization of interacting projectile and target nuclei, (ii) string formation via inelastic nucleon-nucleon (hadron-hadron) interaction, (iii) string fragmentation (i.e., hadronization), and (iv) hadron-hadron rescattering, are solved basically by Monte Carlo simulation techniques.

The results obtained with QGSM are shown in Fig. 7. The time evolution of the densities  $\rho(t)$  and  $\varepsilon(t)$  are qualitatively similar to those obtained with the three models discussed above and quantitatively closest to URQMD for the reason explained above (no repulsion). However, especially at the lower energies, the QGSM expansion trajectories fall significantly below those of the other models.

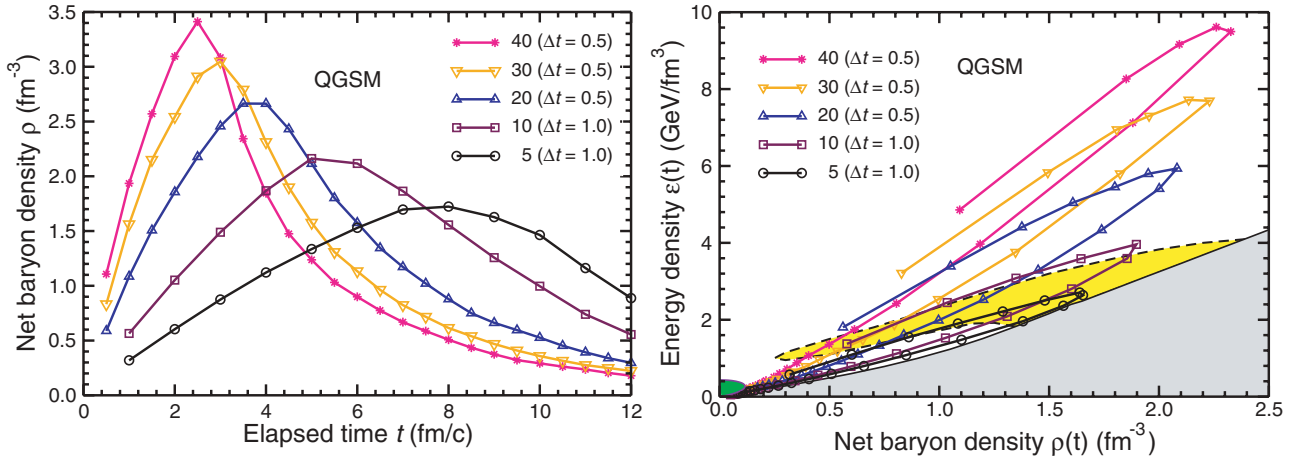


FIG. 7. (Color online) The QGSM evolution of the central net baryon density,  $\rho(t)$  (left), and the corresponding phase trajectory ( $\rho(t)$ ,  $\epsilon(t)$ ) (right) at the center of a head-on Au+Au collision at various bombarding energies (indicated in  $A$  GeV), with the time increments  $\Delta t$  between the symbols indicated in parentheses. Also shown is the schematic reference phase boundary depicted in Fig. 1.

The model assumptions of URQMD and QGSM are rather similar and the absence of hadron repulsion results in higher maximum compressions than those produced by the other models. However, these two models have significantly different expansion dynamics, probably due to larger number of baryonic resonances included in URQMD. As a result of this, the QGSM dynamics are dominated by the propagation of nucleons and pions, whereas URQMD leads to significant resonance production. Because the relatively abundant QGSM pions (which are light) will propagate at velocities much higher than those of the URQMD resonances (which are heavy), they will leave the interaction region earlier, thus causing the energy density to decrease more rapidly than in URQMD. This mechanism is especially important at the lower energies where heavy resonances play a significant role and it gradually subsides as the energy is raised, consistent with the results.

### E. Nuclear Boltzmann equation

The nuclear Boltzmann equation has proven to be quantitatively useful for the description of nuclear collisions at lower energies, up to a few GeV/nucleon, and it may therefore be of interest to employ it also here. For this purpose, we use the Boltzmann-Ühling-Uhlenbeck model developed by the group in Gießen (GiBUU) [38–41].

GiBUU explicitly propagates 9  $N^*$  and 9  $\Delta$  resonances with masses below 2 GeV as well as the  $S = -1$  hyperons  $\Lambda$  and  $\Sigma$  and 19 hyperon resonances; the cascades and charmed baryons are included. The included mesons are  $\pi$ ,  $\eta$ ,  $\rho$ ,  $\sigma$ ,  $\omega$ ,  $\eta'$ ,  $\phi$ ,  $\eta_c$ ,  $J/\psi$ ,  $K$ ,  $\bar{K}$ ,  $K^*$ , and  $\bar{K}^*$ . The baryon-baryon (meson-baryon) collisions below  $\sqrt{s} = 2.6$  GeV are treated within the resonance scenario, whereas the string model is applied above.

Thus GiBUU contains a larger set of the baryonic resonances than most other transport models (excepting URQMD and the Tübingen QMD model) and it consequently leads to higher pion numbers in vacuum. Medium corrections to the cross sections  $NN \leftrightarrow NR$  and  $NN \leftrightarrow NN\pi$  reduce the pion

number in medium. The in-medium reduced cross sections are implemented (optionally) in GiBUU. They are computed with the Dirac masses from the NL2 model [42]. In particular, the  $NN \leftrightarrow N\Delta$  matrix element is given by the one-pion exchange model, as was done in the calculations of Dmitriev *et al.* [43] but with the vacuum  $\Delta$  and nucleon masses replaced by the Dirac values that causes a strong in-medium reduction of the cross section [40].

GiBUU provides a good reproduction of nucleon collective flows [44] as well as pion and kaon multiplicities [40,45], at SIS energies. From AGS to the lower SPS energies, GiBUU overestimates pion multiplicities (with vacuum cross sections) but gives a reasonable description of the kaon multiplicities [41], as do HSD and URQMD. The direct comparison with the HSD and URQMD calculations on the pion and kaon production at 2–40  $A$  GeV [41] has demonstrated that the model yields a somewhat higher  $K^+/\pi^+$  ratio due to additional meson-meson channels in  $K\bar{K}$  production.

GiBUU is suitable not only for nucleus-nucleus and hadron-nucleus collisions but also for photon-, electron-, and neutrino-induced reactions. This gives the possibility of testing the same dynamical part of the model with various physical initial conditions. A new numerical realization of the model [46] is currently being tested.

The results presented here are based on the old version [38,39,41], with the calculations done in the cascade mode, i.e., without a mean field and using vacuum cross sections. These results are shown in Fig. 8. They are rather similar to those obtained with PHSD, the main differences being that GiBUU reaches slightly higher densities and the difference between the outward and the inward trajectory grows somewhat faster as the collision energy is raised.

## V. COMPARISONS

We now compare the phase trajectories obtained with the different models at various collision energies through the

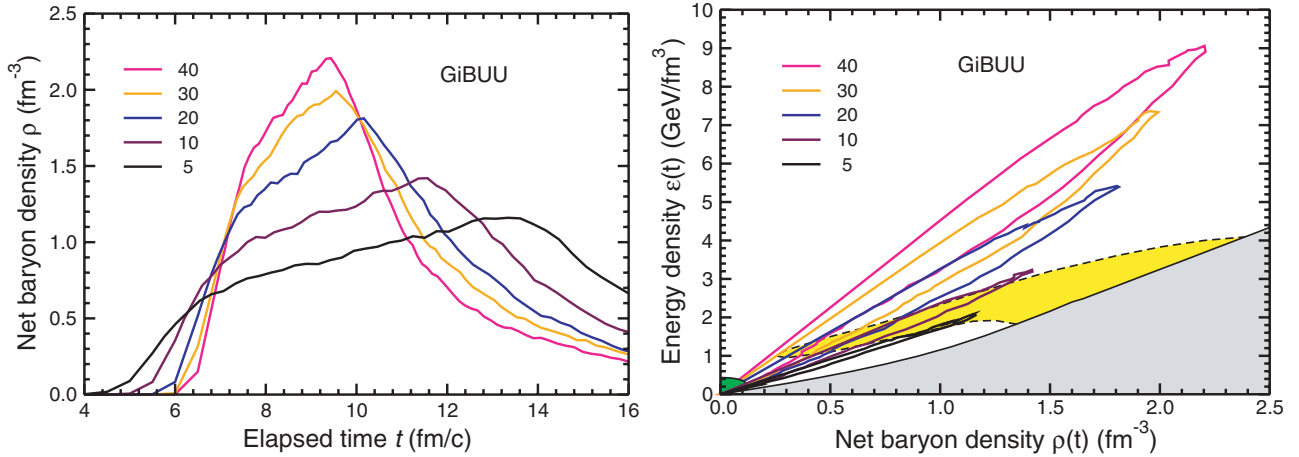


FIG. 8. (Color online) The time evolution of the central net baryon density  $\rho(t)$  (left) and the corresponding phase trajectory ( $\rho(t), \epsilon(t)$ ) (right) at the center of a head-on Au+Au collision at various bombarding energies (indicated in  $A$  GeV), in the GiBUU model, together with the schematic phase boundary shown in Fig. 1.

anticipated FAIR range. These comparisons are shown in Fig. 9 for the beam energies  $E_0 = 5, 10, 20$ , and  $40$  GeV/nucleon.

First, we note that by and large there is a remarkable degree of agreement among the results of the different models. The most notable exception is the QGSM expansion paths, which come out significantly lower than those of the other models, as already discussed in Sec. IV D.

For the subsequent discussion, to make a concrete analysis possible, we take the adopted reference phase boundary at face value. But it is important to keep in mind that this particular boundary, though not inconsistent with any information we presently have, is likely to be quantitatively inaccurate. However, its qualitative form is expected to be correct and our comments below are therefore expected to be robust, provided that appropriate adjustments are made in the specific energy values mentioned.

At the lowest beam energies (under  $5 A$  GeV or so with the adopted phase boundary), the degree of compression and agitation attained does not suffice to bring the central part of the system into the phase coexistence region and such collisions are not likely to have a bearing on the possible existence of a phase transition. However, due to their relative slowness, these collisions achieve of high degree of local equilibrium and the data obtained in this range may well provide quantitative information on the equation of state at the corresponding moderate compressions.

Above those “subthreshold” energies follows a range of beam energies (approximately  $5$ – $10$  GeV/nucleon for the adopted reference phase boundary), within which the highest degree of compression occurs within the region of phase coexistence. As the beam energy is increased through this range, the turning point of the phase trajectory moves across the coexistence region, starting at the hadronic phase coexistence boundary and ending at the plasma boundary. Though somewhat more violent, these trajectories are generally expected to still attain a high degree of local equilibrium. Furthermore, importantly, they spend the longest period of time within the phase coexistence region. Therefore, this energy range appears

to be especially well suited for generating signals of the phase transition.

As the collision energy is increased further, the turning point of the phase trajectory moves further inside the plasma region and, at the same time, the expansion path steepens. The time spent crossing the phase coexistence region then decreases, both in absolute terms and relative to the overall expansion time, so one would expect any phase-transition signals to gradually subside.

Ultimately, beyond a certain critical collision energy (for which the expansion phase trajectory passes straight through the critical point), the phase trajectory never enters the coexistence region but passes entirely to the left of the critical point. Though interesting in its own right, this supercritical region of collision energy would not be expected to elucidate the character of the deconfinement phase transformation, i.e., to help determine whether there is in fact a first-order transition at sufficiently high baryon density.

We also note that the adiabatic expansion results obtained with the SU(3) model correspond approximately to the backtracking of the very early (and mostly nonequilibrium) dynamics when the two Lorentz-contracted nuclear densities are being forced to interpenetrate. This feature mostly reflects the fact that the adopted initial values were taken to reflect such a scenario. If suitably modified initial conditions were chosen, for example, obtained from the turning point of a dynamical trajectory, then the resulting expansion path would exhibit a large degree of resemblance with the corresponding dynamical trajectory. Thus one may characterize the actual dynamical expansions as being approximately adiabatic.

Finally, we wish to emphasize that none of the dynamical models employed (except possibly PHSD) incorporate a first-order phase transition. They would therefore not be suitable, in their present form, for studying actual dynamical consequences of a phase transition. However, the presence of such a phase transition is not expected to have an overwhelming effect on the gross dynamics, primarily due to the predominance of the overall expansion. [This expectation is supported by

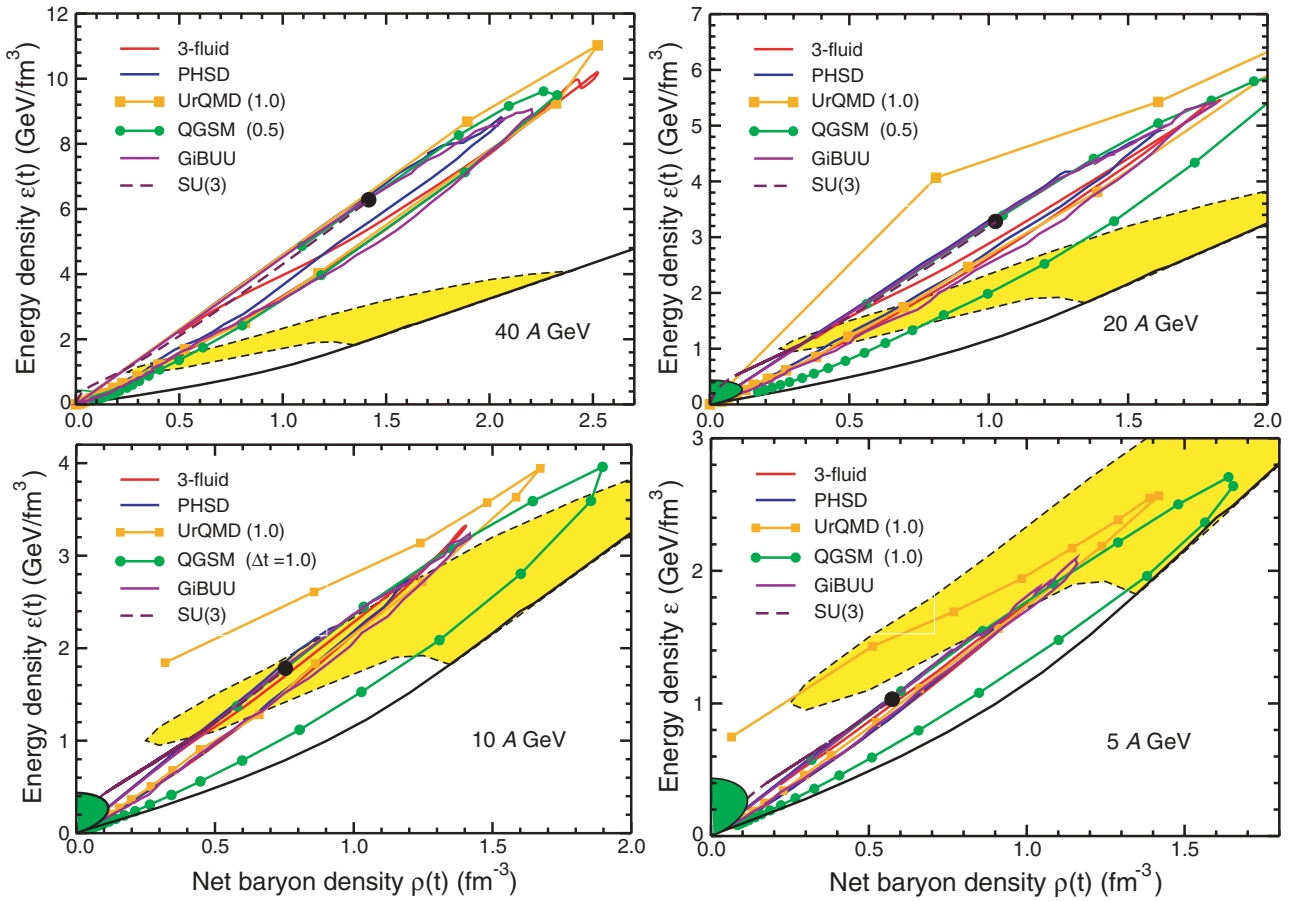


FIG. 9. (Color online) The phase trajectories ( $\rho(t)$ ,  $\epsilon(t)$ ) at the center of a head-on Au+Au collision for various bombarding energies as obtained with the indicated models, together with the schematic phase boundary shown in Fig. 1 and the hadronic freeze-out line [2]. The symbols on the URQMD and QGSM curves are separated by the time intervals indicated in parentheses (fm/c).

comparisons between HSD (which does not contain a partonic phase) and PHSD (which does have a partonic phase) in the energy range considered here.] Therefore, it must also be expected that the effects of a phase transition would be relatively subtle and might best be studied with carefully designed correlation observables.

## VI. CONCLUDING REMARKS

The present study has sought to elucidate the bulk conditions that may be expected to occur in nuclear collisions in the energy range where a possible first-order hadronization phase transition would be encountered. For this we have employed a number of existing dynamical models to central Au+Au collisions and extracted the time evolution of net baryon density  $\rho$  and the energy density  $\epsilon$  at the center of the system where these are expected to achieve their largest values. The different models exhibit a large degree of mutual agreement on the behavior of the corresponding phase trajectories ( $\rho(t)$ ,  $\epsilon(t)$ ), as was summarized in Fig. 9, even if they differ substantially in other regards.

A central issue in the physics of strongly interacting matter is whether the hadronization phase transformation is of first

order at sufficiently high baryon density. The calculation of the corresponding critical point, and the associated phase boundary, poses a significant theoretical challenge and the question may ultimately have to be settled by experiment.

The experimental investigation of this question may employ conceptually different strategies. One strategy searches for the critical point by means of special signals that may occur if the phase trajectory reaches its vicinity. However, the location of the critical point remains theoretically poorly understood and, as is well illustrated by Fig. 9, a small shift in its position would require a relatively large change in the collision energy of the critical phase trajectory that passes through it. Consequently, it is hard to predict what energy range would be most suitable for this approach. Indeed, our present studies cannot rule out that the critical collision energy lies somewhere in the SPS range above the energies reachable by the planned FAIR.

A different experimental strategy seeks direct evidence of the first-order transition by concentrating on signals that might appear as a result of the phase trajectory encountering the phase-transition line. One would expect that such signals would best be generated if the bulk of the system were brought well inside the phase coexistence region, where a phase decomposition is favored, and kept there for a time sufficient to allow the development of the macroscopic nonuniformities

associated with the phase decomposition. Though also associated with significant uncertainties, this issue can probably be assessed with somewhat larger confidence. Thus, considering the large degree of mutual agreement between the different dynamical results and taking first the adopted schematic phase boundary at face value, the present study suggest that the optimal beam energy is around 10 A GeV, corresponding to  $\sqrt{s_{NN}} \approx 2.36 \text{ GeV} + 2.36 \text{ GeV}$  for a collider. We must, however, make allowances for the fact that the adopted schematic phase boundary is not expected to be quantitatively accurate. Furthermore, the dynamical models, though yielding fairly similar results, may all possess common inaccuracies. With a factor of 2 used to account for such uncertainties, the present study would then suggest that the optimal conditions for exploring the hadronization phase transition are likely (though not certain) to occur for beam kinetic energies of 5–20 GeV/nucleon, corresponding to  $\sqrt{s_{NN}} \approx 3.6\text{--}6.4 \text{ GeV}$  for a collider.

These numbers suggest that the planned FAIR at GSI is well matched for such studies. Furthermore, this region may

also be accessible at the low-energy end of RHIC at BNL, as well as at a possible upgraded Nuclotron at JINR in Dubna. Of course, further dynamical studies are required before it is possible to identify the specific candidate signals and to assess whether they can indeed be expected to develop sufficiently even at the optimal collision energy. We hope that this study will provide stimulation in this regard.

#### ACKNOWLEDGMENTS

This work was supported by the Office of Energy Research at the U.S. Department of Energy (DOE contract DE-AC03-76SF00098), the Deutsche Forschungsgemeinschaft (DFG project 436 RUS 113/558/0-3), and the Russian Foundation for Basic Research (RFBR grant 06-02-04001 NNIO\_a), and Russian Federal Agency for Science and Innovations (grant NSh-8756.2006.2). The authors appreciate the hospitality of the Gesellschaft of Schwerionenforschung (GSI) in Darmstadt, where part of this work was carried out, and also acknowledge helpful discussions with K. Gudima.

- 
- [1] R. Stock, J. Phys. G **30**, 633 (2004).  
 [2] C. Adler *et al.* (STAR Collaboration), Phys. Rev. Lett. **86**, 4778 (2001) [Erratum-*ibid.* **90**, 119903 (2003)].  
 [3] Yu. B. Ivanov, V. N. Russkikh, and V. D. Toneev, Phys. Rev. C **73**, 044904 (2006).  
 [4] P. Senger, J. Phys. G **30**, 014904 (2004).  
 [5] F. Karsch, J. Phys. G **30**, S887 (2004).  
 [6] M. Stephanov, K. Rajagopal, and E. Shuryak, Phys. Rev. Lett. **81**, 4816 (1998).  
 [7] Z. Fodor and S. D. Katz, J. High Energy Phys. **04** (2004) 050.  
 [8] G. S. F. Stephans, J. Phys. G **32**, S447 (2006).  
 [9] A. N. Sissakian, A. S. Sorin, and V. D. Toneev, *Searching for the Mixed Phase of Strongly Interacting Matter at the JINR Nuclotron*, 7–9 July 2005 [<http://theor.jinr.ru/meetings/2005/roundtable>].  
 [10] C. Dorso and J. Randrup, Phys. Lett. **B232**, 29 (1989).  
 [11] V. D. Toneev, E. G. Nikonov, B. Friman, W. N. Nörenberg, and K. Redlich, Eur. Phys. J. C **32**, 399 (2003).  
 [12] J. Randrup and J. Cleymans, Phys. Rev. C **74**, 047901 (2006).  
 [13] P. Papazoglou, D. Zschesche, S. Schramm, J. Schaffner-Bielich, H. Stöcker, and W. Greiner, Phys. Rev. C **59**, 411 (1999).  
 [14] D. Zschesche, H. Stöcker, W. Greiner, and S. Schramm, Phys. Rev. C **65**, 064902 (2002).  
 [15] D. Zschesche, G. Zeeb, S. Schramm, and H. Stoecker, J. Phys. G **31**, 935 (2005).  
 [16] S. Schramm, Phys. Rev. C **66**, 064310 (2002).  
 [17] S. Schramm, Phys. Lett. **B560**, 164 (2003).  
 [18] D. Zschesche, G. Zeeb, and S. Schramm [arXiv:nucl-th/0602073].  
 [19] V. N. Russkikh and Yu. B. Ivanov, Phys. Rev. C **74**, 034904 (2006).  
 [20] Yu. B. Ivanov and V. N. Russkikh [arXiv:nucl-th/0607070].  
 [21] W. Cassing, E. L. Bratkovskaya, and S. Juchem, Nucl. Phys. **A674**, 249 (2000).  
 [22] W. Cassing, talk at ECT\* Workshop on *Parton Propagation through Strongly Interacting Matter*, 27 September 2005 [<http://conferences.jlab.org/ECT/program>].  
 [23] A. Peshier and W. Cassing, Phys. Rev. Lett. **94**, 172301 (2005).  
 [24] H. Weber, E. L. Bratkovskaya, W. Cassing, and H. Stöcker, Phys. Rev. C **67**, 014905 (2003).  
 [25] E. L. Bratkovskaya, M. Bleicher, M. Reiter, S. Soff, H. Stöcker, M. van Leeuwen, S. A. Bass, and W. Cassing, Phys. Rev. C **69**, 054907 (2004).  
 [26] E. L. Bratkovskaya, W. Cassing, and H. Stöcker, Phys. Rev. C **67**, 054905 (2003).  
 [27] P. K. Sahu, W. Cassing, U. Mosel, and A. Ohnishi, Nucl. Phys. **A672**, 376 (2000); P. K. Sahu and W. Cassing, Nucl. Phys. **A712**, 357 (2002).  
 [28] E. L. Bratkovskaya, S. Soff, H. Stöcker, M. van Leeuwen, and W. Cassing, Phys. Rev. Lett. **92**, 032302 (2004).  
 [29] S. A. Bass *et al.*, Prog. Part. Nucl. Phys. **41**, 255 (1998).  
 [30] M. Bleicher *et al.*, J. Phys. G **25**, 1859 (1999).  
 [31] B. Andersson, G. Gustafson, and T. Sjöstrand, Nucl. Phys. **B197**, 45 (1982).  
 [32] B. Andersson, G. Gustafson, and B. Soderberg, Z. Phys. C **20**, 317 (1983).  
 [33] N. S. Amelin, K. K. Gudima, and V. D. Toneev, Sov. J. Nucl. Phys. **51**, 1093 (1990); N. S. Amelin, K. K. Gudima, S. Y. Sivoklov, and V. D. Toneev, Sov. J. Nucl. Phys. **52**, 172 (1990); V. D. Toneev, N. S. Amelin, K. K. Gudima, and S. Yu. Sivoklov, Nucl. Phys. **A519**, 463c (1990).  
 [34] N. S. Amelin, L. V. Bravina, L. P. Csernai, V. D. Toneev, K. K. Gudima, and S. Y. Sivoklov, Phys. Rev. C **47**, 2299 (1993).  
 [35] E. E. Zabrodin, C. Fuchs, L. V. Bravina, and A. Faessler, Phys. Rev. C **63**, 034902 (2001); Phys. Lett. **B508**, 184 (2001).  
 [36] G. Baur, J. Bleibel, C. Fuchs, A. Faessler, L. V. Bravina, and E. E. Zabrodin, Phys. Rev. C **71**, 054905 (2005).  
 [37] V. Gribov, Sov. Phys. JETP **26**, 414 (1968); L. V. Gribov, E. M. Levin, and M. G. Ryskin, Phys. Rep. **100**, 1 (1983).  
 [38] M. Effenberger, E. L. Bratkovskaya, and U. Mosel, Phys. Rev. C **60**, 44614 (1999).  
 [39] M. Effenberger, Ph.D. thesis, Universität Giessen, 1999.  
 [40] A. B. Larionov and U. Mosel, Nucl. Phys. **A728**, 135 (2003).  
 [41] M. Wagner, A. B. Larionov, and U. Mosel, Phys. Rev. C **71**, 034910 (2005).

- [42] S. J. Lee, J. Fink, A. B. Balantekin, M. R. Strayer, A. S. Umar, P. G. Reinhard, J. A. Maruhn, and W. Greiner, Phys. Rev. Lett. **57**, 2916 (1986).
- [43] V. Dmitriev, O. Sushkov, and C. Gaarde, Nucl. Phys. **A459**, 503 (1986).
- [44] A. B. Larionov, W. Cassing, C. Greiner, and U. Mosel, Phys. Rev. C **62**, 064611 (2000).
- [45] A. B. Larionov and U. Mosel, Phys. Rev. C **72**, 014901 (2005).
- [46] O. Buss, L. Alvarez-Ruso, P. Mühlich, and U. Mosel, Eur. Phys. J. A **29**, 189 (2006).